# Photocatalytic degradation of pharmaceutically active compounds (PhACs) in urban wastewater treatment plants effluents under controlled and natural solar irradiation using immobilized TiO2

Rueda-Márquez Juan José, Palacios-Villarreal Cassandra, Manzano Manuel, Blanco Eduardo, Ramirez del Solar Mila, Levchuk Irina



**DOI:** 10.1016/j.solener.2020.08.028

# Photocatalytic degradation of pharmaceutically active compounds (PhACs) in urban wastewater treatment plants effluents under controlled and natural solar irradiation using immobilized $TiO_2$

Juan José Rueda-Márquez[1,2*], Cassandra Palacios-Villarreal[2], Manuel Manzano[2], Eduardo Blanco[3], Mila Ramírez del Solar[3], Irina Levchuk[4,2]

[1]*Department of Separation Science, School of Engineering Science, Lappeenranta-Lahti University of Technology LUT, Sammonkatu 12, 50130 Mikkeli, Finland*

[2]*Department of Environmental Technologies, INMAR-Marine Research Institute. Faculty of Marine and Environmental Sciences, University of Cádiz, Poligono Rio San Pedro s/n, Puerto Real, 11510, Cádiz, Spain*

[3]*Departamento Física de la Materia Condensada and Instituto de Microscopía Electrónica y Materiales (IMEYMAT), Universidad de Cádiz, 11510 Puerto Real, Cádiz, Spain*

[4]*Fine Particle and Aerosol Technology Laboratory, Department of Environmental and Biological Sciences, University of Eastern Finland, P.O. Box 1627, FI-70211 Kuopio, Finland*

## Abstract

The degradation of pharmaceutically active compounds (PhACs) under controlled and natural solar irradiation using immobilized $TiO_2$ was studied in model solution and real urban wastewater effluents. The $TiO_2$ coatings were prepared via the sol-gel method with two different configurations, using simple (thin films) and the "sandwich" approach. Prepared coatings were characterized employing X-ray diffraction (XRD), scanning electron microscopy (SEM), ellipsometry and UV-Vis diffuse reflectance spectroscopy. Decomposition of PhACs detected in urban wastewater effluents (diclofenac, carbamazepine, atenolol, propranolol, albuterol, ofloxacin, ciprofloxacin, azithromycin, erythromycin, hydrochlorothiazide, and furosemide) was monitored using Ultra Performance Liquid Chromatography-Triple Quadrupole Mass Spectrometry (UPLC-QqQ-MS/MS). Among detected PhACs three are included in the Watch List (EU Decision 2018/840). The "sandwich" coatings (deposited on frosted support) with the following structure: anatase layer, $TiO_2$ P25 nanoparticles and anatase layer (sealing film) demonstrated the highest photocatalytic activity among all tested $TiO_2$ coatings and were used for elimination of PhACs from real urban wastewater effluents. Photocatalytic treatment of urban

wastewater effluents under controlled and natural solar irradiation led to moderate and high removal (>40%) of all detected PhACs except carbamazepine and atenolol, for which poor removal efficiency was observed (~20%). Some of the PhACs compounds present in wastewater effluents, such as diclofenac, ofloxacin, ciprofloxacin, hydrochlorothiazide and furosemide were sensitive to solar photolysis. The efficiency of solar photocatalytic inactivation of *Escherichia coli* present in urban wastewater effluent was similar to that of solar disinfection (SODIS).

## 1. Introduction

In recent decades, wastewater treatment has become an important issue for the international community due to its economic, environmental and human health implications (Baresel et al., 2015). Various regulations for wastewater treatment have been adopted by different governments (Blöch, 2005, EPA 2002). Most of these regulations focus on traditional effluent limitations such as Biochemical Oxygen Demand ($BOD_5$), Total Suspended Solids (TSS), Chemical Oxygen Demand (COD), nutrients (phosphorus and nitrogen), etc. However, other potentially toxic compounds are present in wastewaters (Roberts and Thomas, 2006). Among these, pharmaceutically active compounds (PhACs) are getting special attention due to their capacity to cause biological effects at very low concentrations (Suárez et al., 2008). Thus, continuous discharge of PhACs to the aquatic environment through urban wastewater treatment plants effluents may seriously affect the aquatic ecosystems (François et al., 2015, Quinn et al., 2009, Quinn et al., 2011). Environmental risks associated with presence of PhACs in secondary wastewater effluent were evaluated (Verlicchi et al., 2012). Such PhACs as antibiotics (erythromycin, ofloxacin, sulfamethoxazole, clarithromycin, amoxicillin, tetracycline and azithromycin), analgesics/anti-inflammatories (ibuprofen and mefenamic acid), psychiatric drugs (fluoxetine, diazepam) and lipid regulators (fenofibric acid, fenofibrate, gemfibrozil) were reported to pose high

environmental risk (Verlicchi et al., 2012). In another study it was demonstrated that mixture of 13 drugs (atenolol, bezafibrate, carbamazepine, cyclophosphamide, ciprofloxacin, furosemide, hydrochlorothiazide, ibuprofen, lincomycin, ofloxacin, ranitidine, salbutamol, and sulfamethoxazole) at ng/L level could inhibit growth of human embryonic cells (Pomati et al., 2006).

The issue of unregulated discharge of contaminants of emerging concern (CECs) was addressed by series of decisions taken by European Union (Directive 2013/39/EU, EU Decision 2015/495, EU Decision 2018/840). Thus, the first Watch List (EU Decision 2015/495) was created and included pollutants, which pose potential risk to aquatic environment and should be monitored in all EU Member States (Sousa et al., 2019). The second Watch List (EU Decision 2018/840) was published in 2018, in which majority of compounds remained, while five substances were eliminated and three added. Compounds included in Watch List are monitored in freshwater. However, urban Wastewater Treatment Plants (UWWTP), which normally operate with a biological treatment, usually do not represent an effective barrier to most PhACs and other emerging pollutants (Suárez et al., 2008). Hence, additional treatment is required to control the release of PhACs and other pollutants present in wastewater effluents to an aquatic environment. Moreover, there is an increasing demand for water reuse for different purposes, such as agricultural irrigation, industrial processes, urbane services, etc. The reuse of biologically treated wastewater requires a tertiary treatment, which strongly depends on the purpose of use. In the best case, governmental legislations have been introduced with a goal to avoid presence or pathogens, hazardous substances and to ensure the biological and chemical security of the user from a direct exposure risk.

Tertiary treatment methods suitable for removal of pathogens and PhACs from urban wastewater effluents including but not limited to adsorption, electrochemical oxidation, membrane filtration, ozonation, advanced oxidation processes (AOPs), etc. (Suárez et al., 2008, Snyder et al., 2007,

Rasalingam et al., 2014). Advanced Oxidation Processes (AOPs) are based on the production of hydroxyl radicals that can inactivate pathogens and oxidize organic pollutants. Among various AOPs, photocatalytic water treatment has gained extensive attention in the last decades as a promising option for the development of environmentally friendly technologies. Solar photocatalysis is an especially attractive option in places like the South of Europe or North America (Mexico and USA), where conditions of high solar irradiation may contribute to efficient wastewater treatment. Theoretical aspects of photocatalysis can be found in excellent scientific works (Ohtani, 2010, Herrmann, 2010, Herrmann, 1999).The most commonly used photocatalyst for removal of harmful compounds from the aqueous environment under UV and solar irradiation is titanium dioxide (in a form of slurry) (Prieto-Rodríguez et al., 2013, Malesic-Eleftheriadou et al., 2019, Moreira et al., 2018, Malato et al., 2016). The advantages of titanium dioxide include its chemical non-toxicity, relatively low cost and high photocatalytic activity. Despite all the advantages, this method has not found many practical applications in real wastewater and water treatment due to difficulties arising when the powder photocatalyst should be separated from treated water. Therefore, immobilizing of photocatalyst on substrates in the form of thin films could significantly simplify the separation procedure and enhance the photocatalytic process.

The goal of this work was to explore the efficiency of immobilized $TiO_2$ for removal of PhACs from model solutions and real wastewater effluents under simulated and natural solar irradiation. The effect of film thickness and type of support on photocatalytic activity of prepared coatings was studied. Moreover, inactivation of *Escherichia coli* in urban wastewater effluents under solar irradiation was performed.

## 2. Materials and Methods

### 2.1. Chemicals

The N-(-4 Hydroxyphenyl) ethanamide was purchased from Sigma Aldrich. The n-butoxide (TBOT) $C_{16}H_{36}O_4Ti$ (98%) and $TiO_2$ (P25, 99.5%) were obtained from Sigma-Aldrich. The acetylacetone $C_5H_8O_2$ (99.5%) was received from MERK. Ethanol $C_2H_6O$ (99.5%) was purchased from Panreac (ITW companies). Methanol (HPLC grade) was received from Scharlau. The solid phase cartridges (Oasis HLB 200 mg) were purchased from Waters Chromatography Europe BV. Analytical standards of measured PhACs were received from suppliers listed elsewhere (Baena-Nogueras et al., 2016).

### 2.2. Deposition of $TiO_2$ thin films and ″sandwich″ structure films on glass tubes

The $TiO_2$ coatings were prepared with two different configurations using simple (thin films) and the "sandwich" approach. In the simple one, a layer of $TiO_2$ was deposited on the external side of glass tubes, according to the methodology described in (Blanco et al., 2015, Blanco et al., 2018). Briefly, $TiO_2$ precursor sol was prepared by hydrolysis of titanium n-butoxide (TBOT) in a solution containing acetylacetone, used as a chelating agent to reduce titanium alkoxide functionality and reactivity, and ethanol, as a solvent. For that purpose, acidified water ($HNO_3$, pH = 1) was added drop wise to this solution under stirring and finally, the solution was diluted with ethanol leading to final molar ratio TBOT:acetylacetone:$H_2O$:EtOH of 1:0.5:2:35. After stirring for one hour at room temperature, sol was kept for ageing for 100 h before to deposition. Sols were kept in the fridge at 4°C and were stable for several months.

In the simple approach, thin films of $TiO_2$ were deposited on high-quality borosilicate glass (BOROFLOAT®33) cylindrical tubes, with a smooth or frosted surface, with 0.03 m external diameter

and 0.25 m length, which were previously cleaned with a surfactant solution in an ultrasonic bath. Dip coating was performed from the precursor sol at precisely controlled withdrawal speed. Fresh films were subsequently dried at 150°C for 30 min. This procedure was repeated until the desired number of layers was reached. Finally, samples were annealed at various temperatures for the period of 1-2 h. The coatings used for photocatalytic experiments were annealed at 500°C as it was found to be optimal. The oven was programmed to raise the temperature of 1°C each min until the desired temperature (500°C) was achieved. In previous papers (Blanco et al., 2015, Blanco et al., 2018) we showed that annealing at this temperature leads to a high degree of anatase crystallization while preserving some porosity and, then, high surface area. Thus, the film obtained by this procedure was called anatase film.

The structure of the coatings prepared according to the "sandwich" approach is shown in Figure 1. The "sandwich" coatings were prepared as follows. Firstly, the external side of the glass tube was coated with $TiO_2$ film (5 layers), prepared as described above (simple configuration). After that, $TiO_2$ P25 nanoparticles (NPs) dispersed in acetylacetone-ethanol solution (4:1 volume ratio, 40 g/L) by high power ultrasonic probe (20KHz) were deposited on the top of anatase thin film. Finally, the coating was sealed with anatase thin film (simple configuration). The $TiO_2$ P25 NPs are a mixture of anatase and rutile phases, so it is expected to be unmodified at applied annealing temperatures. Rutile NPs were prepared by thermal treatment of $TiO_2$ P25 at 900°C.

### 2.3. Characterization of coatings

Morphology of prepared coatings was followed by scanning electron microscopy (SEM) using NOVA NANOSEM 450 scanning microscope. The crystallization process was followed by X-Ray diffraction (XRD) in a Bruker model D8 Advanced Diffractometer using Cu Kα radiation (λ=0.154nm) in the range of 2θ from 15 to 60° with a 0.02°step size. Samples were analyzed at grazing incidence (0.5°) geometry,

for an optimum polycrystalline thin film diffraction, which allows a better resolution of the titania phase peaks above the amorphous substrate halo. For the evaluation of full-width at half-maximum (FWHM), values were corrected for instrument broadening by using the curve registered for a standard reference material (NIST LaB6 660a). Thickness of coatings prepared on glass tubes was extrapolated from values measured for films prepared similarly on flat support. For estimation of the thickness of prepared coatings reflection ellipsometry (PLASMOS SD-2300) was used. Measurements were performed at room temperature and Brewster conditions using a spot size of 2 $mm^2$ and wavelength 632.8 nm.

An optical method for the band gap energy determination is based on UV-Vis diffuse reflectance spectroscopy by applying the Kubelka-Munk (K-M) function (López and Gómez, 2012). The K-M function, F(R), establishes a relationship between absorbed, scattered and diffused reflected light by the sample, and is defined as:

$$F(R) = \frac{(1-R)^2}{2R} \quad (1)$$

where $R$ is the sample diffuse reflectance. These experiments were performed in a Cary 5000 UV-Vis-NIR spectrophotometer equipped with an integrating sphere for the determination of the diffuse reflectance spectra.

## 2.4. Experimental procedures for photocatalytic decomposition of PhACs

### *2.4.1. Decomposition of acetaminophen in model solution under controlled irradiation*

Photocatalytic activity of prepared $TiO_2$ films deposited on glass tubes (fixed photocatalyst) was evaluated using the solar simulator Suntest CPS+ (Atlas Material Testing Technology LLC) equipped with a xenon lamp (Atlas Xe 1500 B-56001794 E2, Figure 2). It should be mentioned that solar simulator was equipped with the optical filter "coated quartz disk" and an additional filter known as "UV

special glass" (Ref. 56052371, Atlas), which was used to filter the excess of UVC radiation and achieve the simulation of solar global radiation (daylight). The total intensity (including UVA and UVB) used in the experiments was 30 $W/m^2$. The annular Pyrex glass reactor (0.20 m length and 0.044 m inner diameter) was used in batch mode with recirculation. Glass tube (0.03 m external diameter and 0.25 m length) coated with photocatalyst was located inside the Pyrex reactor. The irradiated volume and total volume of water in photocatalytic tests were 97 ml and 400 ml, respectively. The ratio of geometrical surface area of $TiO_2$ deposited on glass tubes and illuminated volume of treated water was 1.94 $cm^2/ml$. Samples were taken at time intervals of 0, 30, 60, 120, 180, 240, 300 and 360 min.

Photocatalytic activity of different coatings were evaluated using a model solution of the N-(-4 Hydroxyphenyl) ethanamide (acetaminophen) with the initial concentration of 15 mg/L. The model solution was prepared using ultrapure water (Milli-Q). The concentration of acetaminophen was determined utilizing a Jenway 7315 UV-Visible spectrophotometer ($\lambda_{max}$ = 243 nm). To confirm the degradation of acetaminophen, the chemical oxygen demand (COD) was measured following standard methods (APHA, 2008) with heating block (J. P. Selecta 7471200) and Thermo Scientific Genesys 10 S UV-Visible spectrophotometer.

### *2.4.2. Photocatalytic decomposition of PhACs in urban wastewater effluent under controlled and natural solar irradiation*

The photocatalytic coating with the highest activity was chosen based on experimental results obtained with a model solution under controlled irradiation and used for subsequent experiments with urban wastewater effluent.

The urban wastewater effluent was received from the wastewater treatment plant (WWTP) "El Torno" located in Chiclana de la Frontera (Cádiz, Spain). The current treatment of "El Torno" wastewater

treatment plant consists in physic-chemical process follow by biological treatment (activated sludge). The wastewater effluent is discharged after settling. Considering that transmittance is a critical parameter for photocatalysis process, suspended solids were removed prior to experiments with real wastewater effluent (glass microfiber filters Whatman GF/A, 1.6 µm size pore, 47 mm diameter). Removal of suspended solids (filtration) was applied before all experiments except photocatalytic disinfection test. The pH and conductivity of wastewater was measured using Crison GLP21 pH meter and Crison GLP32 conductimeter, respectively. The concentration of PhACs present in urban wastewater effluent was measured before and after photocatalytic tests as well as SODIS experiment. Samples pre-treatment and analysis were conducted in duplicate following methods reported earlier (Baena-Nogueras et al., 2016). Briefly, Oasis HLB cartridges (200 mg) were used for solid-phase extraction (SPE). The cartridges were conditioned by consequent use of methanol (8 ml) and Milli-Q water (8 ml). After that, fresh samples of wastewater (aliquots of 100 ml) were passed through HLB cartridges at an average speed of 1 ml/min. Subsequent washing (Milli-Q water, 10 ml) and air drying (30 min) of HLB cartridges were performed. After the evaporation of extracts under a nitrogen stream, these were reconstituted in a mixture of methanol and water and filtered through 0.22 µm PTEF filters. The concentration of PhACs in wastewater samples was measured with Bruker EVOQ Elite (Bruker, Billerica, MA) Ultra Performance Liquid Chromatography-Triple Quadrupole Mass Spectrometry (UPLC-QqQ-MS/MS) equipped with C-18 column (100 x 2.1 mm; particle size 2 µm) and electrospray interface. For both, positive and negative, ionization modes the injection volume was 10 µL and a flow rate of 0.4 mL/min. The aqueous mobile phase used for measurements conducted in positive ionization mode was a mixture of 10 mM formic acid and ammonium formate (pH 3.2), while 100% methanol was used as organic mobile phase. The aqueous mobile phase applied for analysis performed in negative ionization mode was 5 mM ammonium acetate/ammonia (pH 8), while the organic mobile phase

consisted of 100% methanol. Multiple reaction monitoring (MRM) was used for data acquisition. Obtained data were processed with Bruker MS Workstation 8.1 Software. More details can be found in (Baena-Nogueras et al., 2016).

*Escherichia coli* was monitored on the course of the photocatalytic tests under natural solar irradiation using the membrane filtration method (APHA, 2008). Wastewater samples were filtered through gridded membranes (0.45 µm, Pall Corporation, NY, USA), plated in Petri dishes containing selective medium and incubated at 37°C for 24 h. Chromogenic Colinstant Agar (Scharlau) was used as a selective agar-based medium for *Escherichia coli* determination. Results were expressed as colony-forming unit (CFU) per 100 ml of water. It should be noted that each sample was analysed in quadruplicate and variation coefficients of mean values were below 30%. A log-linear approach for description of microbial inactivation curves ($N = N_0 \cdot e^{-k \cdot UVDose}$) was applied for *E.coli* inactivation by SODIS and solar photocatalysis. Experimental results were fitted to log-linear approach using GinaFit (Geeraerd et al., 2005) and validated using a coefficient of determination ($R^2 \geq 0.95$) and Root Mean Sum of Squared Error (RMSE, which varied between 0.22 and 0.36).

Experiments with real wastewater effluent were conducted under controlled irradiation conditions and natural solar light. All experiments conducted in controlled irradiation (using model solution or real wastewater effluent) were performed in equipment shows in Figure 2. Characterization of urban wastewater effluent is shown in Table 1.

Figure 3 shows the experimental set up applied for photocatalytic tests with urban wastewater effluent under natural solar irradiation. Experiments were conducted at the University of Cadiz, Campus of Puerto Real (Spain, local latitude 36°31’ N) on sunny days. A Compound Parabolic Collector (CPC) with a reflective surface of 0.08 $m^2$ specifically designed for use of an immobilized photocatalyst on tubular support (Glass Type 3.3, Schott-Duran, 0.4 m length, 0.045 m inner diameter) was used. The

CPC was facing south and inclined 36° (in accordance with the latitude of the location of the experiments). Assays were performed by recirculating the water in continuous batch mode for 360 minutes, using a centrifuge pump (20W, Iwaki, Mod.MD-20R-220N). The irradiated volume inside the reactor was 450 ml, while the total initial volume used for this experiment was 2200 ml. The intensity of solar radiation (UVA and UVB) was measured by employing a radiometer UV34, PCE Iberica, Spain. Cumulative UV dose and normalized time (Malato et al., 2002) were calculated as shown in equations (2) and (3), respectively.

$$Q_{UV,n} = Q_{UV,n-1} + \sum(UV_n \cdot \Delta t) \cdot \frac{V_i}{V_T} \quad (2)$$

where $Q_{UV}$ - cumulative UV dose at each instant (Wh/m$^2$), $UV_n$ - the UV irradiance recorded for each time interval (W/m$^2$), $\Delta t$ - time interval between measurements (h), $V_i$ – illuminated volume (L) of the reactor, $V_T$ – total volume (L) of the reactor.

$$t_{30W,n} = t_{30W,n-1} + \Delta t_n \frac{UV}{30} \frac{V_i}{V_T} \quad (3)$$

where $t_n$- experimental time for each sample, UV – average ultraviolet irradiance measured during the interval $\Delta t_n$, $V_i$ – illuminated volume (L) of the reactor, $V_T$ – total volume (L) of the reactor.

## 3. Results and Discussion

### *3.1. Characterization of prepared coatings*

The annealing temperature for anatase thin films processing was chosen according to two criteria: (i) the elimination of the organic residues after the formation of the oxide gel layer (thermogravimetric analysis and infrared absorption spectra reveal that most of remaining organics are evolved under 500°C as shown in (Blanco et al., 2015) Figures 2 and 3) and (ii) the preservation of the porous structure to increase the surface area (according to Figure 12 in (Blanco et al., 2015, Blanco et al., 2018), Table 3 in

(Blanco et al., 2018) and Figure 6.1 in (Ramirez-del-Solar and Blanco, 2017). The anatase top layer plays a dual role as part of the photocatalyst and as a sealing layer for the lower P25 layer. For this purpose, it is important to clean and preserve the porous network of the gel. In a previous work (Blanco et al., 2015) we have showed that after annealing at 500°C chemical residua from gel synthesis have been removed from the pores and high porosity of the anatase film was preserved. Thus, this cleaning step allows to obtain an active and stable photocatalytic material free from organic groups. Moreover, high porosity allows efficient interaction between the photocatalyst and the adsorbed pollutants (Ramirez-del-Solar and Blanco, 2017).

Figure 4 shows the XRD profiles, registered under grazing incidence, for one layer (thickness approx. 50 nm) of gel deposited on a flat microscope glass and treated at 500°C and 550°C. The characteristic anatase (1,0,1) peak at 25.4° appears very intense and narrow, while other anatase peaks, like (2,0,0) and (0,0,4) can also be distinguished. In fact, it was showed (Blanco et al., 2018) that anatase is the only phase visible for any film treated below 750°C and evaluation of the crystallites size from the (1,0,1) peak broadening and position indicates that annealing at 500 - 550°C leads to average crystallite sizes close to 20 nm.

Scanning electron micrographs of anatase thin films and "sandwich" coatings are shown in Figure 5. From Figure 5 (A), a 40 nm anatase film on the bottom (indicated using an arrow) and a larger (>2μm) P25 layer can be distinguished.

For the "sandwich" approach an important requirement for the sealant layer is that it does not hinder the P25 photocatalytic activity by absorbing suitable radiation. Thus, the optical bandgap energy of the anatase gel layer was evaluated and compared with that of P25 film. Figure 6 shows F(R) functions obtained for sol-gel $TiO_2$ annealed at different temperatures in the range 400 - 800ºC, measured directly

from the diffuse reflectance detected with the spectrophotometer integrating sphere. Although this method has been frequently applied to highly light scattering materials and absorbing particles in a matrix, it is also possible to apply it to particulate coatings that both scatters and absorbs light (Murphy, 2007). Thus, the basic K–M model assumes the diffuse illumination of the granular structure where surfaces are optically rough as it is shown by our $TiO_2$ thin films and evidenced by AFM and SEM results (Blanco et al., 2018). A modification of the K–M model allows its application in the case of collimated illumination (Murphy, 2006). Thus, if E is the photon energy, the Tauc method can be applied to the function $(F(R)\cdot E)^n$ versus E, with n=1/2 for indirect semiconductors (López and Gómez, 2012), will presents a linear region where the relationship $(F(R)\cdot E)^{1/2} = k\cdot(E-E_g)$ applies. In this way, the bandgap energy of semiconductor nanocrystals,$E_g$, can be obtained from the extrapolation to zero of the linear regions of the plots (Figure 6, inset).

The $E_g$-KM values obtained in this way are plotted in Figure 7, they are smaller values than those obtained from a Tauc-Lorentz model applied to spectroscopy ellipsometry results (Blanco et al., 2018) but they follow the same trend with the annealing temperature. The imaginary part of the Tauc-Lorentz dielectric function is established through multiplying the equation of the classical Lorentz oscillator by the expression of the Tauc joint density of states (Jellison and Modine, 1996):

$$\varepsilon_2 = \frac{AE_{(n_0)}C(E_n-E_g)^2}{(E_n-E_{(n_0)}^2)^2+C^2E_n^2}\frac{1}{E_n} \quad (E_n > E_g) \tag{4}$$

$$\varepsilon_2 = 0 \quad (E_n \le E_g) \tag{5}$$

where $A$ is the amplitude, $E_{n_0}$ is the peak position, $C$ is the broadening parameter, and $E_g$ is the TL optical gap.

The equation for the real part, $\varepsilon_1$, can be derived using the Kramers-Kronig integration. It should be noted that the TL model includes only interband transitions; any defect absorption, intraband absorption, or Urbach tail absorption is explicitly ignored in it. Although, due to the empirical nature of the TL model, usually reproduces the experimental data very well even below the optical band gap, the compromise between the two components of the TL model results in the modification of the nominal band gap (TL gap) relative to the true optical band gap $E_g$, when the TL model fits to real data. The TL gap is in this sense a mathematical gap rather than a real physical one. Kubelka-Munk method based on diffuse reflectance measurements allows to obtain the value of the optical band gap from an equation similar to the Tauc relation. It has been already reported that the band gap retrieved from the Kubelka-Munk method showed lower values than that obtained from SE analysis through the TL model but they follow a similar trend in both cases (Goswami and Sharma, 2019).

In Figure 7 three regions can be distinguished: bellow 350°C, where the film is mainly amorphous and only very small crystallites would exist, if any (amorphous region); the region in the range 350 - 800°C, where mainly anatase crystal are present (anatase region); and, finally, above 800°C where some rutile crystals are detected (rutile region). If we focus on the anatase region, we can see how the gap energy decreases when the annealed temperature increases, for all used procedures to determine $E_g$. The upper anatase layer, with a higher energy gap than the P25 layer underlying it, is transparent in the lower energy region, corresponding to the P25 gap. It can be expected that the radiation of 3.3 - 3.1 eV would be transmitted through the small thickness of the anatase film and reach the P25 layer. A transmittance of P25 layer compared with that of an anatase layer is shown in Figure 8.

### *3.2. Photocatalytic decomposition of acetaminophen under controlled irradiation*

#### *3.2.1. Effect of thin film thickness on photocatalytic activity*

It is well documented that as the mass of photocatalyst increase so does the photocatalytic activity up to a certain point, which is strongly dependant on operational conditions and reactor geometry (Kowalska et al., 2010). Usually, the loading of photocatalytic material increases proportionally as the thickness of the film increases (Gregori et al., 2014). Therefore, it is important to study the effect of film thickness on photocatalytic reaction rates. This was performed using anatase thin films with different thickness and photocatalytic decomposition of acetaminophen from model solution was evaluated. In order to estimate the degradation of acetaminophen by photolysis, a blank glass substrate was set instead of thin film and experiments were conducted in a defined order. No significant changes in acetaminophen concentration as a result of adsorption were observed during experiments conducted without irradiation for 360 min. The results of photocatalytic acetaminophen decomposition by anatase thin films deposited on smooth glass tubes with different thickness are presented in Figure 9.

As shown in Figure 9 and Table 2, the lowest values of acetaminophen removal were achieved by photolysis. The removal efficiency of acetaminophen was increased when photocatalytic thin films were used. As the thickness of the film increases (up to 180 nm) so does photocatalytic activity. Thus, initial reaction rate was 2 times higher when coating with thickness 180 nm was used in comparison with 100 nm. This can be attributed to the fact that with increase of film thickness higher amount of $TiO_2$ is available for generation of free radicals. Taking into consideration porosity of prepared anatase films, water can be in contact with inner surface of the gel, thus increasing the photocatalytic activity. Further increase of film thickness (from 180 to 290 nm) leads to decrease of photocatalytic activity. Thus, initial reaction rate of anatase films (270 and 290 nm) was about 20% lower than that of optimal thickness (180 nm). This can be explained by the fact that once an optimal thickness is reached, the process may begin to be mass-transfer limited, so that the useful surface of the photocatalyst does not increase even though the thickness of the layer growths. Obtained results are in agreement with the study of Gregori et al.

(Gregori et al., 2014), in which authors reported that photocatalytic activity of $TiO_2/SiO_2$ thin films strongly increased with the increase of film thickness up to 300 nm, while in the interval from 300 to 900 nm only slight increase was observed. It should be noted that in the study of Gregori et al. the surface morphology was similar for thin films with different thickness (Gregori et al., 2014). However, when surface properties (roughness, grain size, morphology, etc.) of thin films with different thickness varies significantly the thickness of the coating is not playing a crucial role on the photocatalytic activity as reported in earlier studies (Singh et al., 2017).

Several studies were conducted in order to determine the dependence between film thickness and photocatalytic activity (Vilhunen and Sillanpää, 2009, Tada and Tanaka, 1997, Jung et al., 2005, Fallet et al., 2006, Langlet et al., 2003). In some of these studies critical film thickness, the value after which an increase of thickness will not lead to the increase of photocatalytic activity was reported. For instance, in (Eufinger et al., 2008) effect of $TiO_2$ thin film thickness on photocatalytic activity was described and critical thickness was evaluated as 350 nm. In (Jung et al., 2005) the highest photocatalytic activity was detected at film thickness between 1 and 5 μm, further increase in thickness did not enhance photodecomposition of methylene blue. However, considering results presented in (Jung et al., 2005) one should take into account that surface morphology of thin films is varying with different thickness, thus not only thickness of films possibly affects changes in photocatalytic activity.

### *3.2.2. Effect of substrate on photocatalytic activity*

Thin films of anatase with thickness of 270 and 290 nm were deposited on smooth and frosted glass tubes in order to check the effect of substrate on photocatalytic properties of coatings. The results are shown in Figure 10A and Table 2.

As shown in Figure 10A, the initial reaction rates of anatase thin films deposited on a frosted substrate were higher than that of similar coatings deposited on smooth glass. Thus, the initial degradation rate of acetaminophen was about 1.8 times higher when anatase thin films with a thickness of 270 and 290 nm were deposited on frosted glass. The increase of photocatalytic activity of anatase thin films deposited on frosted glass can be attributed to a higher surface roughness of frosted glass in comparison with the smooth one. This allows increasing the surface roughness of the thin films (Figure 5C), which leads to an increase of photocatalytic activity. Roughness of frosted glass is also expected to improve the gel film adherence. Obtained results are in an agreement with a few studies showing an increase of thin film photocatalytic activity with the rise of surface roughness (Lee et al., 2010, Medina-Valtierra et al., 2007).

As indicated in Figure 10B and Table 2, a significant increase of photocatalytic activity was observed when "sandwich" $TiO_2$ coatings (except for rutile) were used in comparison with anatase thin films. Thus, initial reaction rate of ″sandwich″ coating (P25) deposited on smooth glass was about 2.8 times higher in comparison with optimal anatase coating (180 nm) deposited on smooth glass. These results can possibly be explained by different morphology of the film and higher thickness of "sandwich" $TiO_2$ coatings (> 1μm, P25). In ″sandwich″ approach, the NPs of P25 were fixed and sealed by a porous anatase film that can contribute to photocatalytic activity while preserving the P25 layer and allowing water to its interior through the porous network. Moreover, Degussa (Evonik) P25 NPs are well known for relatively high photocatalytic activity and it is often used as ″standard″ photocatalyst. $TiO_2$ P25 contains anatase and rutile crystallites, some authors reported presence of amorphous phase (Ohno et al., 2001, Ohtani et al., 2010). For instance, in excellent work of Ohtani et al. the ratio anatase:rutile:amorphous of P25 was found to be 78:14:8 (Ohtani et al., 2010). The question of high photocatalytic activity of $TiO_2$ P25 was addressed by a few studies (Ohno et al., 2001, Ohtani et al.,

2010, Bickley et al., 1991, Martin et al., 1994, Emilio et al., 2006). Bickley et al. (Bickley et al., 1991) suggested that rutile forms thin overlayer on some anatase particles of P25, which leads to enhanced photocatalytic activity. Later Datye et al. (Datye et al., 1995) reported separate presence of single crystal particles of anatase and rutile in P25. Results obtained by Onho et al. (Ohno et al., 2001) were not in agreement with (Bickley et al., 1991), which was attributed to different sample preparation. Onho et al. (Ohno et al., 2001) observed separate existence of anatase and rutile phases were in P25, which is in agreement with (Datye et al., 1995), and suggested that high photocatalytic activity of P25 can be attributed contact of anatase and rutile particles under practical operational conditions (when agglomerates of anatase and rutile are decomposed). Hurum et el. (Hurum et al., 2003) reported that presence of small rutile crystallites in P25 creates a structure where rapid electron transfer from rutile to lower energy anatase lattice trapping sites under visible illumination leads to a more stable charge separation. However, Ohtani et el. (Ohtani et al., 2010) reported that anatase, rutile and amorphous phase of Degussa P25 work independently and effect of inert-particle interaction on photocatalytic activity of P25 (if any) was insignificant. These results (Ohtani et al., 2010) suggest absence of synergetic effect due to co-presense of anatase and rutile in Degussa P25.

The "sandwich" $TiO_2$ coatings (P25) deposited on smooth and frosted glass tubes were tested for decomposition of acetaminophen. The "sandwich" $TiO_2$ coatings were prepared using rutile and P25 (a combination of anatase and rutile) NPs. As it can be seen from Figure 10B and Table 2, the photocatalytic activity of rutile was about six times lower than that of "sandwich" coating containing P25 NPs. This observation is in agreement with a general understanding and supported by an excellent study (Prieto-Mahaney et al., 2009).

Judging from Figure 10B, it appears that the initial decomposition rate of acetaminophen (estimated for UV dose 24.9 $Wh/m^2$) was about 1.5 times higher for the "sandwich" $TiO_2$ (P25) coating deposited on

frosted glass tube as compared to one deposited on smooth glass. Thus, the highest photocatalytic activity was observed for the "sandwich" $TiO_2$ coatings (P25) deposited on frosted glass. The decomposition of organic pollutants present in model solution was confirmed by monitoring of COD values during the photocatalytic test with "sandwich" $TiO_2$ coatings (P25) deposited on frosted glass (Figure 11). Thus, about 50% of COD removal was observed for acetaminophen model solution and more than 60% of COD removal for urban wastewater effluent under controlled irradiation.

### *3.3. Photocatalytic decomposition of PhACs in urban wastewater effluent under controlled and natural solar radiation*

The "sandwich" $TiO_2$ (P25) coating deposited on frosted glass tube was used for the photocatalytic treatment of urban wastewater effluents due to higher photocatalytic activity among all tested coatings. Concentrations of PhACs present in urban wastewater effluents, namely, diclofenac, carbamazepine, atenolol, propranolol, albuterol, ofloxacin, ciprofloxacin, azithromycin, erythromycin, hydrochlorothiazide and furosemide were measured before and after photocatalytic tests conducted both under natural sunlight and controlled irradiation. It should be noted that PhACs present in wastewater and/or natural waters might be sensitive to photodegradation (photolysis) under solar radiation (Baena-Nogueras et al., 2017). Hence, the concentration of PhACs was also measured after the reference test (photolysis under natural solar light). The initial concentration of PhACs in urban wastewater effluents used for photocatalytic tests under controlled and natural solar irradiation varied (Table 1). Thus, higher initial concentration of almost all PhACs (except azithromycin) was detected in effluent treated under controlled irradiation (*suntest* equipment). The efficiency of photocatalytic treatment for removal of PhACs from urban wastewater effluents is presented in Figure 12.

PhACs, such as carbamazepine, atenolol, propanolol, albuterol, azithromycin and erythromycin, were removed by photocatalysis under controlled or natural solar irradiation to different degrees (21.5 – 99.5%), while no degradation was detected for all abovementioned compounds under solar photolysis. Measured concentrations of carbamazepine in urban wastewater effluent were higher than those reported earlier (Moreira et al., 2015, Prieto-Rodríguez et al., 2013, Prieto-Rodriguez et al., 2012). A rather low removal efficacy of carbamazepine was obtained by photocatalysis under controlled (26.8%; 55 Wh/$m^2$; $t_{30W}$ 110 min) and natural solar (21.5%; 33 Wh/$m^2$; $t_{30W}$ 66 min) irradiation. Such poor removal efficiency of carbamazepine can possibly be attributed to low sorption capacity of carbamazepine as relatively polar, neutrally charged compound (Clara et al., 2004, Scheytt et al., 2006, Ternes et al., 2002). Thus, no sorption of carbamazepine on the surface of N-doped $TiO_2$ was reported after 60 min of contact time (Avisar et al., 2013). Moreover, negative effect of wastewater matrix on elimination of carbamazepine was reported in scientific literature. For, instance, complete suppression of photocatalytic carbamazepine removal in comparison with groundwater and surface water was reported (Avisar et al., 2013), which was attributed to relatively high concentration of natural organic matter and alkalinity (as $CaCO_3$) of wastewater effluent. Resistance of carbamazepine to solar photocatalysis was reported by (Miranda-García et al., 2011). Complete degradation of carbamazepine was not achieved after $t_{30W}$ above 120 min (Miranda-García et al., 2011), which is in agreement with our results. It should be mentioned that almost complete removal of carbamazepine (initial concentration 417 ng/L) was reported when $TiO_2$ (P25 Degussa; 0.2 g/L) was used for solar photocatalytic treatment of wastewater effluent when amount of accumulated UV energy was 32 kJ/L (Sousa et al., 2012). Taking into consideration that in our study the amount of UV energy (experiments conducted under natural solar irradiation) was about 8 times lower than that in (Sousa et al., 2012), it can be expected that it was not sufficient for complete decomposition of carbamazepine. Thus, roughly 37% of carbamazepine was removed from

wastewater effluent in work of (Sousa et al., 2012) when accumulated UV energy was similar to that in our study (experiments conducted under natural solar irradiation). Interestingly, carbamazepine was persistent under solar photolysis (0% of removal; 75 Wh/$m^2$), which agrees with an earlier study (Baena-Nogueras et al., 2017). About 67 – 74% of carbamazepine (initial concentration varied between 151 and 391 ng/L) elimination from wastewater effluents was reported to be reached after solar photolysis during five consecutive days (mean irradiance 25 – 32 W/$m^2$).

Atenolol (β-blocker) is one of the most widely used compounds against cardiovascular diseases (Arvand et al., 2008). Atenolol concentrations detected in wastewater effluents subjected to solar photocatalysis were similar to those reported in (Prieto-Rodríguez et al., 2013). At applied doses, photocatalytic reduction of atenolol concentration was relatively low under controlled (25.7%; 55 Wh/$m^2$; $t_{30W}$ 110 min) and natural (20.3%; 33 Wh/$m^2$; $t_{30W}$ 66 min) solar irradiation. It should be mentioned that reactive sites of atenolol are an activated aromatic ring and secondary amine-moiety. Among reactive sites of atenolol, reaction of amine-moiety ($pK_a$ 9.6) depends on pH (7.46) of the solution (Hapeshi et al., 2010). Hence, it can be expected that amino group could be protonated. The point of zero charge of $TiO_2$ usually varies from 5 to 6.6 (Kosmulski, 2002). Thus, in case if water pH is higher than point of zero charge, the surface of $TiO_2$ becomes negatively charged (Hapeshi et al., 2010). As a result, electrostatic attraction between surface of photocatalyst and atenolol should theoretically lead to high conversion of atenolol by photocatalysis, which is opposite to observed results. There might be a few possible reasons for that. It should be taken into account that wastewater effluent is complex matrix, containing natural organic carbon and various species that may act as radical scavengers. Thus, it was demonstrated in the literature (Hapeshi et al., 2010) that decomposition of atenolol significantly decrease when performed in wastewater matrix in comparison with ultrapure water. Another important parameter which should be taken into consideration is UV dose. Thus, the UV dose was relatively low in experiments under

controlled (55 Wh/m$^2$; $t_{30W}$ 110 min) and natural solar irradiation (33 Wh/m$^2$, $t_{30W}$ 66 min). Consulting the scientific literature (Prieto-Rodríguez et al., 2013), when similar initial concentration of atenolol in wastewater effluents was detected, solar heterogeneous photocatalysis with $TiO_2$ was not efficient for degradation of atenolol even after $t_{30W}$ 475 min, which is in agreement with our results. It can be expected that atenolol decomposition by photocatalysis requires higher UV dose. The solar photolysis did not cause a decrease of atenolol concentration, which is in agreement with (Baena-Nogueras et al., 2017). Obtained results are in agreement with earlier studies (Prieto-Rodriguez et al., 2012), in which atenolol present in urban wastewater effluent was not decomposed completely by solar photocatalysis with $TiO_2$ (slurry, 0.2 g/L) even after $t_{30W}$ 475 min.

Relatively low initial concentrations of propanolol were observed in tested wastewater effluents (10.3 – 14.7 ng/L), which is in agreement with (Prieto-Rodriguez et al., 2012). The removal efficiency of propanolol by photocatalysis was relatively high under both, controlled (79.6%; 55 Wh/m$^2$; $t_{30W}$ 110 min) and natural solar irradiation (63.1%; 33 Wh/m$^2$; $t_{30W}$ 66 min), while no degradation was observed by solar photolysis. Similar behaviour was observed in the case of albuterol. Thus, high removal efficiencies were observed for albuterol for solar photocatalysis (77.4 – 88.7%), while no elimination was detected during photolysis, which is in agreement with (Baena-Nogueras et al., 2017).

Higher removal of azithromycin and erythromycin, compounds included in Watch List by EU Decision 2018/840, was observed in case of solar photocatalysis (87.2% and 99.4%, respectively; 33 Wh/m$^2$; $t_{30W}$ 66 min) as compared to photocatalysis under controlled irradiation (51.8% and 43.1%, respectively; 55 Wh/m$^2$; $t_{30W}$ 110 min), while the initial concentrations were very similar for both wastewater effluents. Taking into account that in case of photocatalysis under controlled irradiation the cumulative UV dose was higher than for solar photocatalysis, the removal of azithromycin and erythromycin was lower, which can be possibly attributed to differences in the solar emission spectra and that of Xenon lamp.

Concentrations of azithromycin and erythromycin were not decreased after solar photolysis. According to the literature (Tong et al., 2011), about 70% of azithromycin (initial concentration 20 µg/L) in a river water matrix was degraded by day nine under natural solar irradiation. The half-life of three–ten days weas reported for macrolides, including erythromycin, under simulated solar light in natural waters (Batchu et al., 2014).

Removal efficiencies obtained during photocatalysis under both simulated and natural solar irradiations for diclofenac, ofloxacin, ciprofloxacin, hydrochlorothiazide, and furosemide were rather high (61.4 – 100%). However, it should be stressed that these compounds were susceptible to decomposition under solar irradiation in the absence of photocatalyst although at a lower speed. Diclofenac concentrations detected in wastewater effluents were similar to those reported by (Villar-Navarro et al., 2018) for urban wastewater effluents. Almost complete elimination of diclofenac was achieved by photocatalysis performed under controlled (97.6%; 55 $Wh/m^2$; $t_{30W}$ 110 min) and natural (100%; 33 $Wh/m^2$; $t_{30W}$ 66 min) solar irradiation. Immobilized $TiO_2$ was successfully applied for photocatalytic removal of diclofenac and other pollutants from real wastewaters under solar irradiation and lead to 90% of removal at $t_{30W}$ 32.80 min (Miranda-García et al., 2011). Prieto-Rodriguez et al. (Prieto-Rodriguez et al., 2012) reported that $t_{30W}$ required for an almost complete elimination of diclofenac (4425 ng/L) from wastewater effluents by $TiO_2$ (slurry, 0.02 g/L) under natural solar light was below 300 min, which is in agreement with results obtained in our study. However, in another study (Prieto-Rodríguez et al., 2013) even higher $t_{30W}$ was reported for the elimination of diclofenac from urban wastewater effluents by solar $TiO_2$ photocatalysis (slurry, 0.02 g/L). Interestingly, very high removal efficiency (90%; 75 $Wh/m^2$) of diclofenac was achieved by photolysis under natural solar radiation, which is in agreement with earlier studies (Pérez-Estrada et al., 2005). Thus, almost complete (99%) decomposition of diclofenac in model solution (initial concentration 100 ng/L) was reported (Baena-Nogueras et al., 2017) under simulated

solar irradiation (*suntest*) during 24 h, which can be possibly explained by significantly higher UV dose. Some studies demonstrated that the elimination rate of diclofenac increased during photocatalysis as compared to photolysis (Salaeh et al., 2016). However, it should be noted that these studies were conducted with concentrations of diclofenac significantly higher than concentrations usually found in real urban wastewater effluents (Salaeh et al., 2016).

High removal efficiency of ofloxacin and ciprofloxacin was achieved by solar photolysis (78.6 and 89.3%, respectively; 75 Wh/m$^2$; $t_{30W}$ 150 min) as well as photocatalysis under controlled (69.1 and 61.4%, respectively; 55 Wh/m$^2$; $t_{30W}$ 110 min) and natural solar irradiation (84.8 and 93.5%, respectively; 33 Wh/m$^2$; $t_{30W}$ 66 min). It should be noted that ciprofloxacin is included in Watch List by EU Decision 2018/840. According to the literature, 90% of ofloxacin (initial concentration 100 µg/L in real wastewater effluent) was achieved by solar photocatalysis (immobilized $TiO_2$) after $t_{30W}$ 22.72 min, which increased up to 32.36 min after five cycles (Miranda-García et al., 2011). Hydrochlorothiazide was detected at the highest concentrations (4005.4 – 5049.9 ng/L) among all studied PhACs in wastewater effluents and it was about 4 - 5 times higher than reported earlier (Prieto-Rodríguez et al., 2013). Very high levels of hydrochlorothiazide removal were achieved after photocatalysis under natural (96.6%; 33 Wh/m$^2$; $t_{30W}$ 66 min) and controlled irradiation (82.3%; 55 Wh/m$^2$; $t_{30W}$ 110 min), which is in agreement with results reported earlier (Prieto-Rodríguez et al., 2013, Moreira et al., 2015, Prieto-Rodriguez et al., 2012, Sousa et al., 2012). It should be noticed that solar photolysis was very efficient for hydrochlorothiazide decomposition (95%; 75 Wh/m$^2$; $t_{30W}$ 150 min) as well, which is in agreement with (Baena-Nogueras et al., 2017). Similar results were observed for furosemide. It should be noticed that as shown in Figure 11B, the COD significantly decreases in the case of photocatalysis, while it is not the case during photolysis as it was demonstrated in earlier studies (Levchuk et al., 2015).

### *3.4. Solar photocatalytic inactivation of E.coli in urban wastewater effluents*

Photocatalytic solar disinfection experiments were performed using "sandwich" $TiO_2$ (P25) coating deposited on frosted glass tube as it demonstrated the highest photocatalytic activity for removal of the organic pollutants from model water. Inactivation of *E.coli*, which is often used as an indicator microorganism, was monitored on the course of the experiments. Initial concentration of *E.coli* in wastewater (not filtered) was $3 \cdot 10^5$ CFU/100 mL. Solar disinfection (in absence of photocatalyst) and so-called dark test (in absence of solar radiation and in the presence of photocatalyst) was performed as a reference tests. Results of *E.coli* inactivation are shown as Log ($N/N_0$) *vs* Dose ($Wh/m^2$) in Figure 13.

As it can be seen from Figure 13, inactivation of *E.coli* using "sandwich" $TiO_2$ (P25) coating under solar irradiation ($k_{max}$ = 0.23 ± 0.03 $m^2/Wh$; $R^2$ = 0.95; RMSE = 0.3592) was very similar to SODIS ($k_{max}$ = 0.27 ± 0.02 $m^2/Wh$; $R^2$ = 0.98; RMSE = 0.2219), while no inactivation was observed in dark test. Obtained results are in agreement with earlier studies (Levchuk et al., 2018), in which photocatalytic thin films were used for *E.coli* inactivation under natural solar light. However, for $TiO_2$ in form of slurry (Helali et al., 2014), significant increase of *E.coli* inactivation was reported as compared to SODIS. Moreover, often when photocatalyst is used bacteria regrowth can be avoided (Fernández et al., 2005).

**Conclusions**

In this study photocatalytic activity of immobilized $TiO_2$ coatings (thin anatase and "sandwich" films) was tested under controlled and natural solar irradiation in model solution and real urban wastewater effluents. Photocatalytic inactivation of *E.coli* under natural solar irradiation was also studied. The main outcomes of this study are presented below.

- Coatings (thin anatase and "sandwich" films) deposited on frosted substrates led to higher photocatalytic activity.

- The "sandwich" coatings (deposited on frosted support) with the following structure: anatase layer, $TiO_2$ P25 nanoparticles and anatase layer (sealing film) demonstrated the highest photocatalytic activity among all tested $TiO_2$ coatings and were used for elimination of PhACs from real urban wastewater effluents.
- Photocatalytic treatment of urban wastewater effluents under controlled and natural solar irradiation led to significant removal of all detected PhACs except carbamazepine and atenolol. Some of the PhACs present in wastewater effluents, such as diclofenac, ofloxacin, ciprofloxacin, hydrochlorothiazide and furosemide were sensitive to solar photolysis. However, the use of photocatalyst allowed to increase the number of PhACs that can be decomposed (in comparison with solar irradiation without photocatalyst) and to reach significant COD reduction of wastewater effluent, which indicates greater degradation of PhACs and not only loss of the original structure.
- The efficiency of solar photocatalytic inactivation of *Escherichia coli* present in urban wastewater effluent was similar to that of solar disinfection (SODIS). However, regrowth prevention and inactivation of microorganisms with lower sensitivity to solar irradiance are among main advantages of introducing photocatalytic materials to solar water disinfection.

**Acknowledgments**

This research was partially supported by SUNRAS PROJECT (Project AGL2016-80507-R) funded by Ministerio de Economia y Competitividad (Plan Nacional de I+D+i (2013-2016)). Dr. Rueda-Marquez is grateful for financial support from Academy of Finland within the project ″Combination of Advanced Oxidation Processes and Photobiotreatment for Sustainable Resource Recovery and Wastewater Reuse″ (№322339, 2019 - 2022).

## References


APHA, A., WPCF, 2008. Standard Methods for the Examination of Water and Wastewater.

Arvand, M., Vejdani, M., Moghimi, M., 2008. Construction and performance characterization of an ion selective electrode for potentiometric determination of atenolol in pharmaceutical preparations. Desalination 225, 176-184.

Avisar, D., Horovitz, I., Lozzi, L., Ruggieri, F., Baker, M., Abel, M., Mamane, H., 2013. Impact of water quality on removal of carbamazepine in natural waters by N-doped $TiO_2$ photo-catalytic thin film surfaces. J. Hazard. Mater. 244, 463-471.

Baena-Nogueras, R.M., González-Mazo, E., Lara-Martín, P.A., 2017. Degradation kinetics of pharmaceuticals and personal care products in surface waters: photolysis vs biodegradation. Science of The Total Environment 590-591, 643-654.

Baena-Nogueras, R.M., Pintado-Herrera, M.G., Gonzalez-Mazo, E., Lara-Martin, P.A., 2016. Determination of Pharmaceuticals in Coastal Systems Using Solid Phase Extraction (SPE) Followed by Ultra Performance Liquid Chromatography - tandem Mass Spectrometry (UPLC-MS/MS). Current Analytical Chemistry 12, 183-201.

Baresel, C., Palm Cousins, A., Ek, M., Ejhed, H., Allard, A.-S., Magnér, J., Westling, K., Fortkamp, U., Wahlberg, C., Hörsing, M., Söhr, S., 2015. Pharmaceutical residues and other emerging substances in the effluent of sewage treatment plants. Review on concentrations, quantification, behaviour, and removal options. B 2226.

Batchu, S.R., Panditi, V.R., O'Shea, K.E., Gardinali, P.R., 2014. Photodegradation of antibiotics under simulated solar radiation: implications for their environmental fate. Sci. Total Environ. 470, 299-310.

Bickley, R.I., Gonzalez-Carreno, T., Lees, J.S., Palmisano, L., Tilley, R.J.D., 1991. A structural investigation of titanium dioxide photocatalysts. Journal of Solid State Chemistry 92, 178-190.

Blanco, E., Domínguez, M., González-Leal, J., Márquez, E., Outón, J., Ramírez-del-Solar, M., 2018. Insights into the annealing process of sol-gel $TiO_2$ films leading to anatase development: The interrelationship between microstructure and optical properties. Appl. Surf. Sci. 439, 736-748.

Blanco, E., González-Leal, J., Ramírez-del Solar, M., 2015. Photocatalytic $TiO_2$ sol–gel thin films: optical and morphological characterization. Solar Energy 122, 11-23.

Blöch, H., 2005. European Union legislation on wastewater treatment and nutrients removal.

Clara, M., Strenn, B., Kreuzinger, N., 2004. Carbamazepine as a possible anthropogenic marker in the aquatic environment: investigations on the behaviour of carbamazepine in wastewater treatment and during groundwater infiltration. Water Res. 38, 947-954.

Datye, A.K., Riegel, G., Bolton, J.R., Huang, M., Prairie, M.R., 1995. Microstructural Characterization of a Fumed Titanium Dioxide Photocatalyst. Journal of Solid State Chemistry 115, 236-239.

Emilio, C.A., Litter, M.I., Kunst, M., Bouchard, M., Colbeau-Justin, C., 2006. Phenol photodegradation on platinized-$TiO_2$ photocatalysts related to charge-carrier dynamics. Langmuir 22, 3606-3613.

EPA, 2002. FEDERAL WATER POLLUTION CONTROL ACT. , 1-234.

Eufinger, K., Poelman, D., Poelman, H., De Gryse, R., Marin, G.B., 2008. $Ti0_2$ thin films for photocatalytic applications, in S.C. Nam (Ed.), Thin Solid Films: Process and Applications, pp. 189-227.

Fallet, M., Permpoon, S., Deschanvres, J.L., Langlet, M., 2006. Influence of physico-structural properties on the photocatalytic activity of sol-gel derived TiO2 thin films. J. Mater. Sci. 41, 2915-2927.

Fernández, P., Blanco, J., Sichel, C., Malato, S., 2005. Water disinfection by solar photocatalysis using compound parabolic collectors. Catalysis Today 101, 345-352.

François, G., Mélanie, D., Marlène, F., Michel, F., 2015. Effects of a municipal effluent on the freshwater mussel Elliptio complanata following challenge with Vibrio anguillarum. Journal of Environmental Sciences 37, 91-99.

Geeraerd, A., Valdramidis, V., Van Impe, J., 2005. GInaFiT, a freeware tool to assess non-log-linear microbial survivor curves. Int. J. Food Microbiol. 102, 95-105.

Goswami, S., Sharma, A.K., 2019. Investigation of the optical behavior of indium oxide thin films with the aid of spectroscopic ellipsometry technique. Appl. Surf. Sci. 495, 143609.

Gregori, D., Benchenaa, I., Chaput, F., Therias, S., Gardette, J., Léonard, D., Guillard, C., Parola, S., 2014. Mechanically stable and photocatalytically active $TiO_2/SiO_2$ hybrid films on flexible organic substrates. Journal of Materials Chemistry A 2, 20096-20104.

Hapeshi, E., Achilleos, A., Vasquez, M.I., Michael, C., Xekoukoulotakis, N.P., Mantzavinos, D., Kassinos, D., 2010. Drugs degrading photocatalytically: Kinetics and mechanisms of ofloxacin and atenolol removal on titania suspensions. Water Research 44, 1737-1746.

Helali, S., Polo-López, M.I., Fernández-Ibáñez, P., Ohtani, B., Amano, F., Malato, S., Guillard, C., 2014. Solar photocatalysis: A green technology for *E. coli* contaminated water disinfection. Effect of concentration and different types of suspended catalyst. J. Photochem. Photobiol. A. 276, 31-40.

Herrmann, J., 2010. Fundamentals and misconceptions in photocatalysis. J. Photochem. Photobiol. A. 216, 85-93.

Herrmann, J., 1999. Heterogeneous photocatalysis: fundamentals and applications to the removal of various types of aqueous pollutants. Catalysis Today 53, 115-129.

Hurum, D.C., Agrios, A.G., Gray, K.A., Rajh, T., Thurnauer, M.C., 2003. Explaining the enhanced photocatalytic activity of Degussa P25 mixed-phase $TiO_2$ using EPR. The Journal of Physical Chemistry B 107, 4545-4549.

Jellison Jr, G., Modine, F., 1996. Parameterization of the optical functions of amorphous materials in the interband region. Appl. Phys. Lett. 69, 371-373.

Jung, S., Kim, S., Imaishi, N., Cho, Y., 2005. Effect of $TiO_2$ thin film thickness and specific surface area by low-pressure metal–organic chemical vapor deposition on photocatalytic activities. Applied Catalysis B: Environmental 55, 253-257.

Kosmulski, M., 2002. The significance of the difference in the point of zero charge between rutile and anatase. Adv. Colloid Interface Sci. 99, 255-264.

Kowalska, E., Mahaney, O.O.P., Abe, R., Ohtani, B., 2010. Visible-light-induced photocatalysis through surface plasmon excitation of gold on titania surfaces. Phys.Chem.Chem.Phys. 12, 2344-2355.

Langlet, M., Kim, A., Audier, M., Guillard, C., Herrmann, J., 2003. Liquid phase processing and thin film deposition of titania nanocrystallites for photocatalytic applications on thermally sensitive substrates. J. Mater. Sci. 38, 3945-3953.

Lee, W.K., Kim, E.J., Hahn, S.H., 2010. Structural and photocatalytic properties of $TiO_2/SiO_x/TiO_x$ multi-layer prepared by electron-beam evaporation method. Vacuum 85, 30-33.

Levchuk, I., Rueda-Márquez, J., Suihkonen, S., Manzano, M., Sillanpää, M., 2015. Application of UVA-LED based photocatalysis for plywood mill wastewater treatment. Separation and Purification Technology 143, 1-5.

Levchuk, I., Kralova, M., Rueda-Márquez, J.J., Moreno-Andrés, J., Gutiérrez-Alfaro, S., Dzik, P., Parola, S., Sillanpää, M., Vahala, R., Manzano, M.A., 2018. Antimicrobial activity of printed composite $TiO_2/SiO_2$ and $TiO_2/SiO_2$/Au thin films under UVA-LED and natural solar radiation. Applied Catalysis B: Environmental 239, 609-618.

López, R., Gómez, R., 2012. Band-gap energy estimation from diffuse reflectance measurements on sol–gel and commercial $TiO_2$: a comparative study. J. Sol Gel Sci. Technol. 61, 1-7.

Malato, S., Blanco, J., Cáceres, J., Fernández-Alba, A.R., Agüera, A., Rodríguez, A., 2002. Photocatalytic treatment of water-soluble pesticides by photo-Fenton and $TiO_2$ using solar energy. Catalysis Today 76, 209-220.

Malato, S., Maldonado, M.I., Fernández-Ibáñez, P., Oller, I., Polo, I., Sánchez-Moreno, R., 2016. Decontamination and disinfection of water by solar photocatalysis: The pilot plants of the Plataforma Solar de Almeria. Materials Science in Semiconductor Processing 42, 15-23.

Malesic-Eleftheriadou, N., Evgenidou, E.N, Kyzas, G.Z., Bikiaris, D.N., Lambropoulou, D.A., 2019. Removal of antibiotics in aqueous media by using new synthesized bio-based poly (ethylene terephthalate)-$TiO_2$ photocatalysts. Chemosphere 234, 746-755.

Martin, S.T., Herrmann, H., Choi, W., Hoffmann, M.R., 1994. Time-resolved microwave conductivity. Part 1.—$TiO_2$ photoreactivity and size quantization. Journal of the Chemical Society, Faraday Transactions 90, 3315-3322.

Medina-Valtierra, J., Frausto-Reyes, C., Ramírez-Ortíz, J., Moctezuma, E., Ruiz, F., 2007. Preparation of rough anatase films and the evaluation of their photocatalytic efficiencies. Applied Catalysis B: Environmental 76, 264-274.

Miranda-García, N., Suárez, S., Sánchez, B., Coronado, J.M., Malato, S., Maldonado, M.I., 2011. Photocatalytic degradation of emerging contaminants in municipal wastewater treatment plant effluents using immobilized TiO2 in a solar pilot plant. Applied Catalysis B: Environmental 103, 294-301.

Moreira, N.F.F., Narciso-da-Rocha, C., Polo-López, M.I., Pastrana-Martínez, L.M., Faria, J.L., Manaia, C.M., Fernández-Ibáñez, P., Nunes, O.C., Silva, A.M.T., 2018. Solar treatment ($H_2O_2$, $TiO_2$-P25 and GO-$TiO_2$ photocatalysis, photo-Fenton) of organic micropollutants, human pathogen indicators, antibiotic resistant bacteria and related genes in urban wastewater. Water Research 135, 195-206.

Moreira, N.F.F., Orge, C.A., Ribeiro, A.R., Faria, J.L., Nunes, O.C., Pereira, M.F.R., Silva, A.M.T., 2015. Fast mineralization and detoxification of amoxicillin and diclofenac by photocatalytic ozonation and application to an urban wastewater. Water Research 87, 87-96.

Murphy, A., 2007. Band-gap determination from diffuse reflectance measurements of semiconductor films, and application to photoelectrochemical water-splitting. Solar Energy Mater. Solar Cells 91, 1326-1337.

Murphy, A., 2006. Modified Kubelka–Munk model for calculation of the reflectance of coatings with optically-rough surfaces. J. Phys. D 39, 3571.

Ohno, T., Sarukawa, K., Tokieda, K., Matsumura, M., 2001. Morphology of a $TiO_2$ Photocatalyst (Degussa, P-25) Consisting of Anatase and Rutile Crystalline Phases. Journal of Catalysis 203, 82-86.

Ohtani, B., Prieto-Mahaney, O., Li, D., Abe, R., 2010. What is Degussa (Evonik) P25? Crystalline composition analysis, reconstruction from isolated pure particles and photocatalytic activity test. J. Photochem. Photobiol. A. 216, 179-182.

Ohtani, B., 2010. Photocatalysis A to Z—What we know and what we do not know in a scientific sense. Journal of Photochemistry and Photobiology C: Photochemistry Reviews 11, 157-178.

Pérez-Estrada, L.A., Maldonado, M.I., Gernjak, W., Agüera, A., Fernández-Alba, A.R., Ballesteros, M.M., Malato, S., 2005. Decomposition of diclofenac by solar driven photocatalysis at pilot plant scale. Catalysis Today 101, 219-226.

Pomati, F., Castiglioni, S., Zuccato, E., Fanelli, R., Vigetti, D., Rossetti, C., Calamari, D., 2006. Effects of a complex mixture of therapeutic drugs at environmental levels on human embryonic cells. Environ. Sci. Technol. 40, 2442-2447.

Prieto-Mahaney, O., Murakami, N., Abe, R., Ohtani, B., 2009. Correlation between photocatalytic activities and structural and physical properties of titanium (IV) oxide powders. Chem. Lett. 38, 238-239.

Prieto-Rodriguez, L., Miralles-Cuevas, S., Oller, I., Agüera, A., Puma, G.L., Malato, S., 2012. Treatment of emerging contaminants in wastewater treatment plants (WWTP) effluents by solar photocatalysis using low $TiO_2$ concentrations. J. Hazard. Mater. 211, 131-137.

Prieto-Rodríguez, L., Oller, I., Klamerth, N., Agüera, A., Rodríguez, E.M., Malato, S., 2013. Application of solar AOPs and ozonation for elimination of micropollutants in municipal wastewater treatment plant effluents. Water Research 47, 1521-1528.

Quinn, B., Gagné, F., Blaise, C., 2009. Evaluation of the acute, chronic and teratogenic effects of a mixture of eleven pharmaceuticals on the cnidarian, Hydra attenuata. Science of The Total Environment 407, 1072-1079.

Quinn, B., Schmidt, W., O'Rourke, K., Hernan, R., 2011. Effects of the pharmaceuticals gemfibrozil and diclofenac on biomarker expression in the zebra mussel (Dreissena polymorpha) and their comparison with standardised toxicity tests. Chemosphere 84, 657-663.

Ramirez-del-Solar, M., Blanco, E., 2017. Porous Thin Films from Sol-Gel, in Anonymous Submicron Porous Materials. Springer, pp. 157-188.

Rasalingam, S., Peng, R., Koodali, R.T., 2014. Removal of hazardous pollutants from wastewaters: applications of $TiO_2$-$SiO_2$ mixed oxide materials. Journal of Nanomaterials 2014, 10.

Roberts, P.H., Thomas, K.V., 2006. The occurrence of selected pharmaceuticals in wastewater effluent and surface waters of the lower Tyne catchment. Sci. Total Environ. 356, 143-153.

Salaeh, S., Perisic, D.J., Biosic, M., Kusic, H., Babic, S., Stangar, U.L., Dionysiou, D.D., Bozic, A.L., 2016. Diclofenac removal by simulated solar assisted photocatalysis using $TiO_2$-based zeolite catalyst; mechanisms, pathways and environmental aspects. Chem. Eng. J. 304, 289-302.

Scheytt, T.J., Mersmann, P., Heberer, T., 2006. Mobility of pharmaceuticals carbamazepine, diclofenac, ibuprofen, and propyphenazone in miscible-displacement experiments. J. Contam. Hydrol. 83, 53-69.

Singh, J., Khan, S.A., Shah, J., Kotnala, R., Mohapatra, S., 2017. Nanostructured $TiO_2$ thin films prepared by RF magnetron sputtering for photocatalytic applications. Appl. Surf. Sci. 422, 953-961.

Snyder, S.A., Adham, S., Redding, A.M., Cannon, F.S., DeCarolis, J., Oppenheimer, J., Wert, E.C., Yoon, Y., 2007. Role of membranes and activated carbon in the removal of endocrine disruptors and pharmaceuticals. Desalination 202, 156-181.

Sousa, M., Gonçalves, C., Vilar, V.J., Boaventura, R.A., Alpendurada, M., 2012. Suspended TiO2-assisted photocatalytic degradation of emerging contaminants in a municipal WWTP effluent using a solar pilot plant with CPCs. Chem. Eng. J. 198, 301-309.

Sousa, J.C.G., Ribeiro, A.R., Barbosa, M.O., Ribeiro, C., Tiritan, M.E., Pereira, M.F.R., Silva, A.M.T., 2019. Monitoring of the 17 EU Watch List contaminants of emerging concern in the Ave and the Sousa Rivers. Sci. Total Environ. 649, 1083-1095.

Suárez, S., Carballa, M., Omil, F., Lema, J.M., 2008. How are pharmaceutical and personal care products (PPCPs) removed from urban wastewaters? Reviews in Environmental Science and Bio/Technology 7, 125-138.

Tada, H., Tanaka, M., 1997. Dependence of $TiO_2$ photocatalytic activity upon its film thickness. Langmuir 13, 360-364.

Ternes, T.A., Meisenheimer, M., McDowell, D., Sacher, F., Brauch, H., Haist-Gulde, B., Preuss, G., Wilme, U., Zulei-Seibert, N., 2002. Removal of pharmaceuticals during drinking water treatment. Environ. Sci. Technol. 36, 3855-3863.

Tong, L., Eichhorn, P., Pérez, S., Wang, Y., Barceló, D., 2011. Photodegradation of azithromycin in various aqueous systems under simulated and natural solar radiation: Kinetics and identification of photoproducts. Chemosphere 83, 340-348.

Verlicchi, P., Al Aukidy, M., Zambello, E., 2012. Occurrence of pharmaceutical compounds in urban wastewater: Removal, mass load and environmental risk after a secondary treatment—A review. Sci. Total Environ. 429, 123-155.

Vilhunen, S., Sillanpää, M., 2009. Atomic layer deposited (ALD) $TiO_2$ and $TiO_{2-x}$-$N_x$ thin film photocatalysts in salicylic acid decomposition. Water Science and Technology 60, 2471-2475.

Villar-Navarro, E., Baena-Nogueras, R.M., Paniw, M., Perales, J.A., Lara-Martín, P.A., 2018. Removal of pharmaceuticals in urban wastewater: High rate algae pond (HRAP) based technologies as an alternative to activated sludge based processes. Water Res. 139, 19-29.


**Figure 1.** Schematic presentation of $TiO_2$ coatings with "sandwich" structure

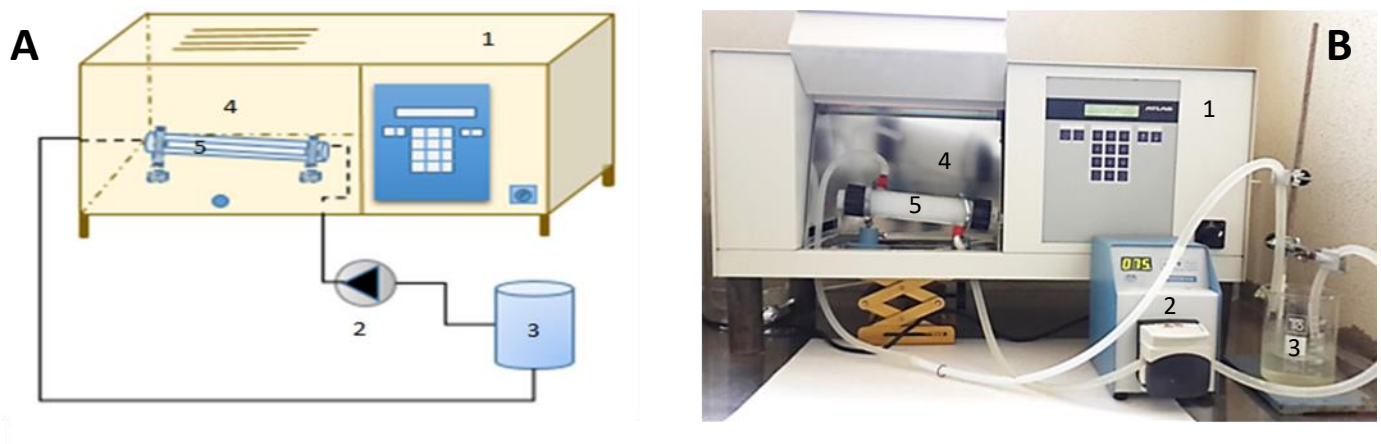


**Figure 2.** Schematic representation (A) and photo (B) of the experimental set up for photocatalytic experiments under controlled irradiation. 1 - solar simulator; 2 - peristaltic pump; 3 – reservoir; 4 – tubular reactor; 5 – tube coated with photocatalyst

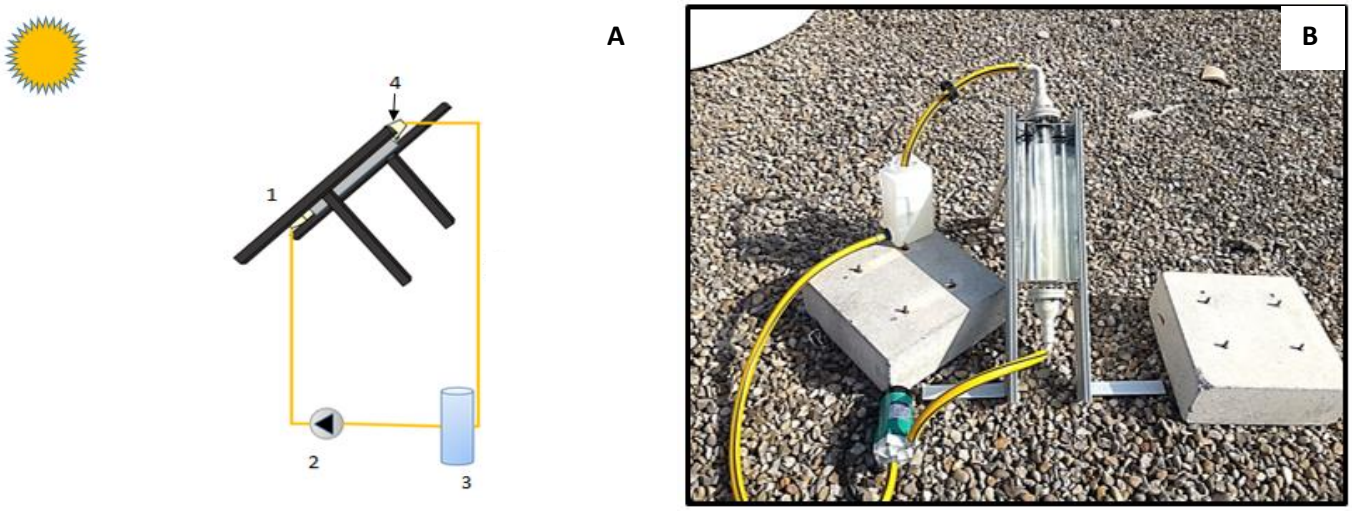


**Figure 3.** Scheme (A) and photo (B) of experimental set up for solar photocatalytic experiments with urban wastewater. 1 - Compound Parabolic Collector (CPC); 2 - peristaltic pump; 3 – reservoir; 4 – photocatalyst.

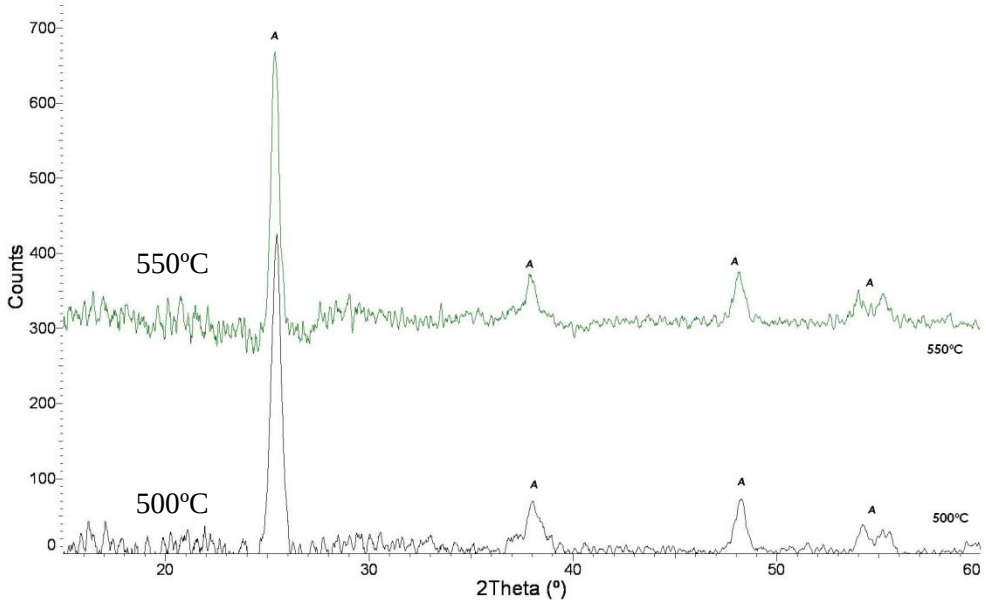


**Figure 4.** XRD profiles of anatase thin films annealed at 500ºC and 550 ºC

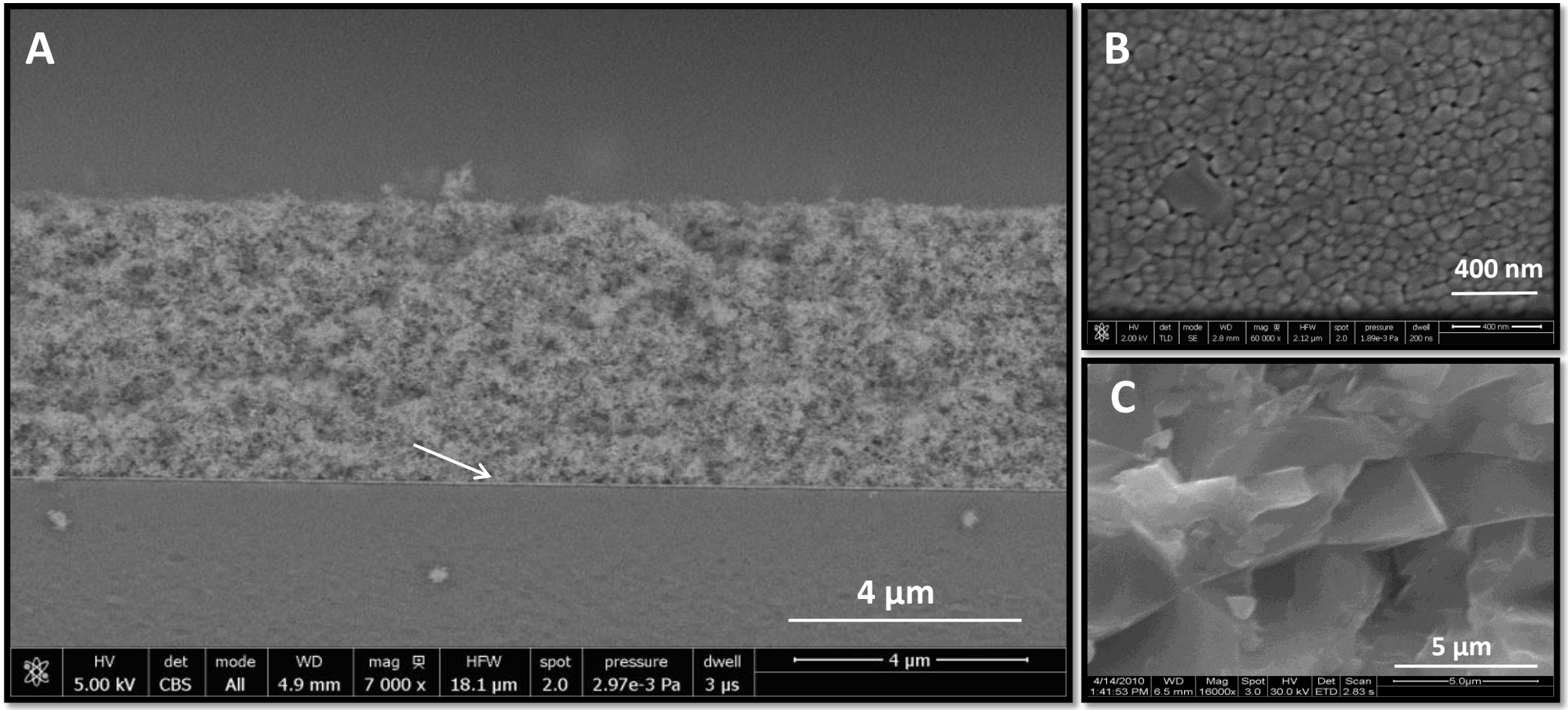


**Figure 5.** Scanning electron microscopic (SEM) micrograph of the "sandwich" type coating (A), anatase thin film (B) and surface of frosted glass used as support for the photocatalytic thin films (C)

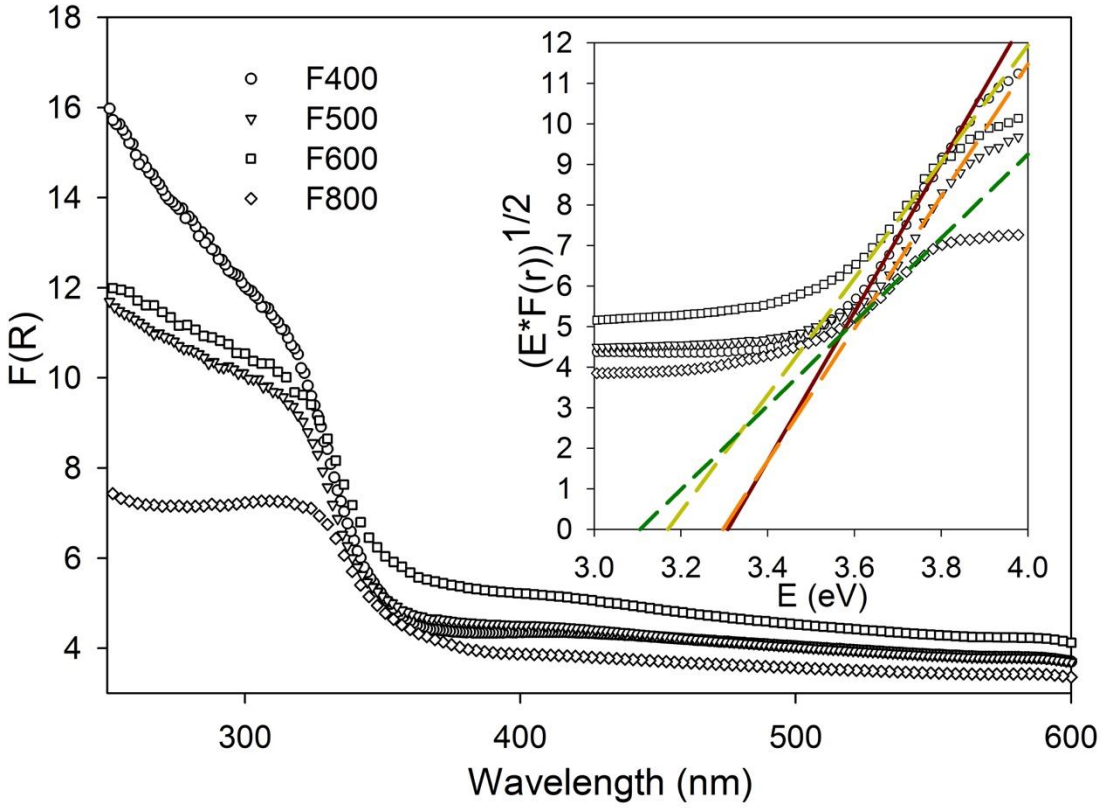


**Figure 6.** F(R) functions obtained for anatase thin films annealed at different temperatures in the range 400 - 800ºC

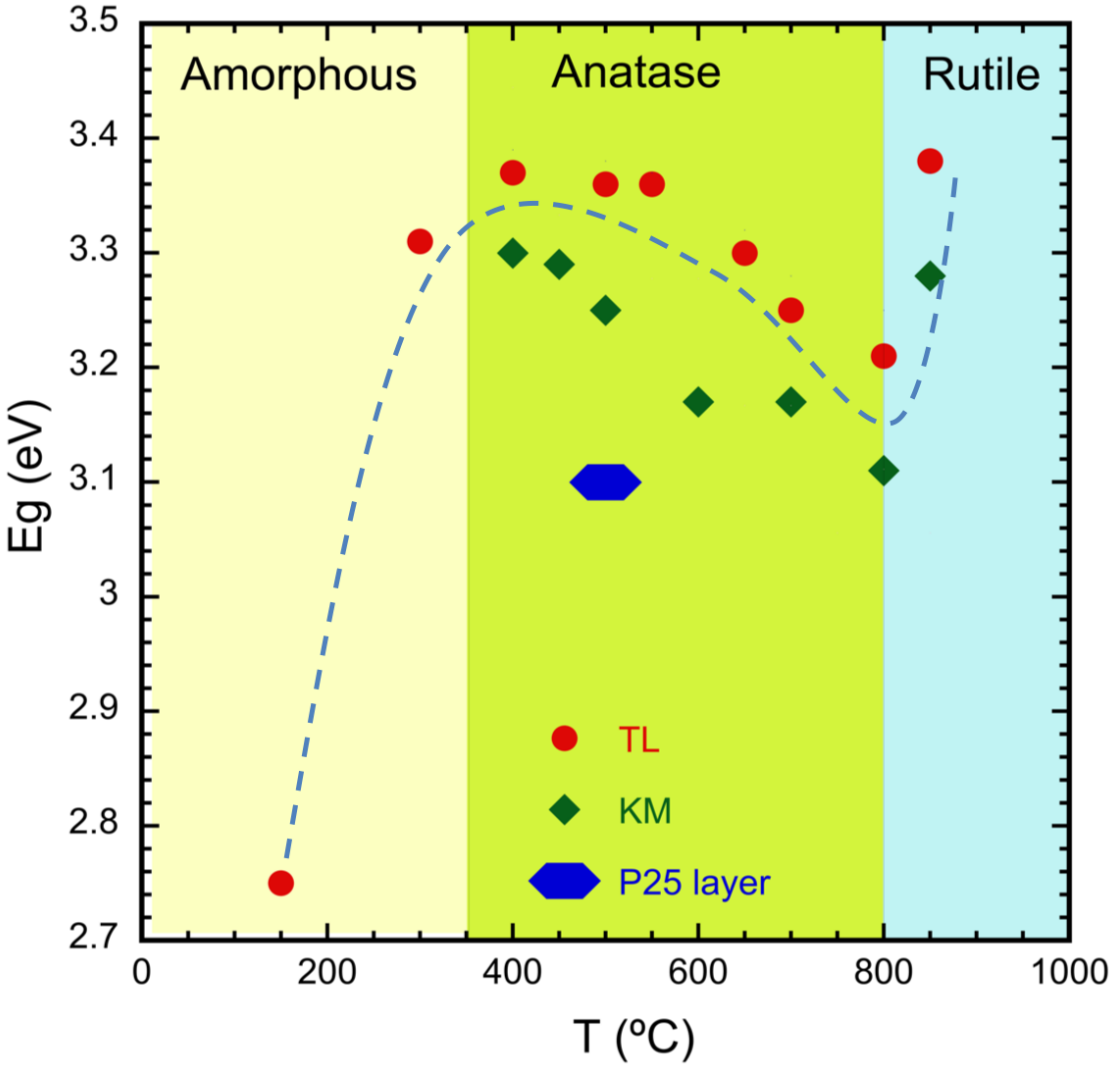


**Figure 7.** Band gap energy of $TiO_2$ coatings annealed at different temperatures. Band gap energy was determined using Kubelka-Munk function (KM) and Tauc-Lorentz model (TL)

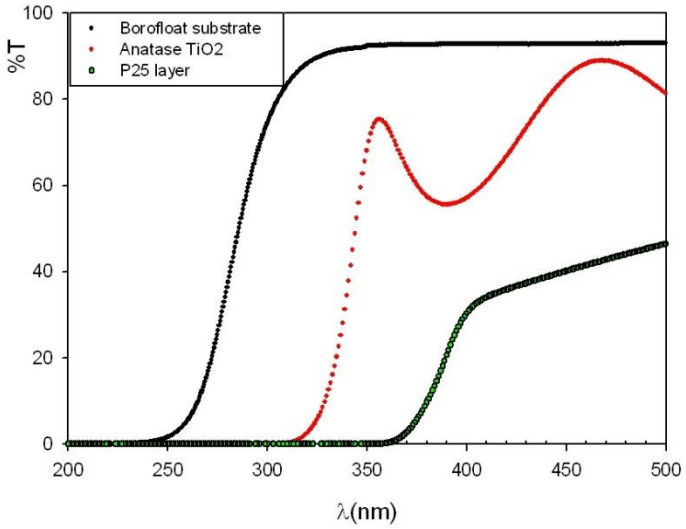


**Figure 8.** Comparison of transmittance of anatase film (red) and P25 film

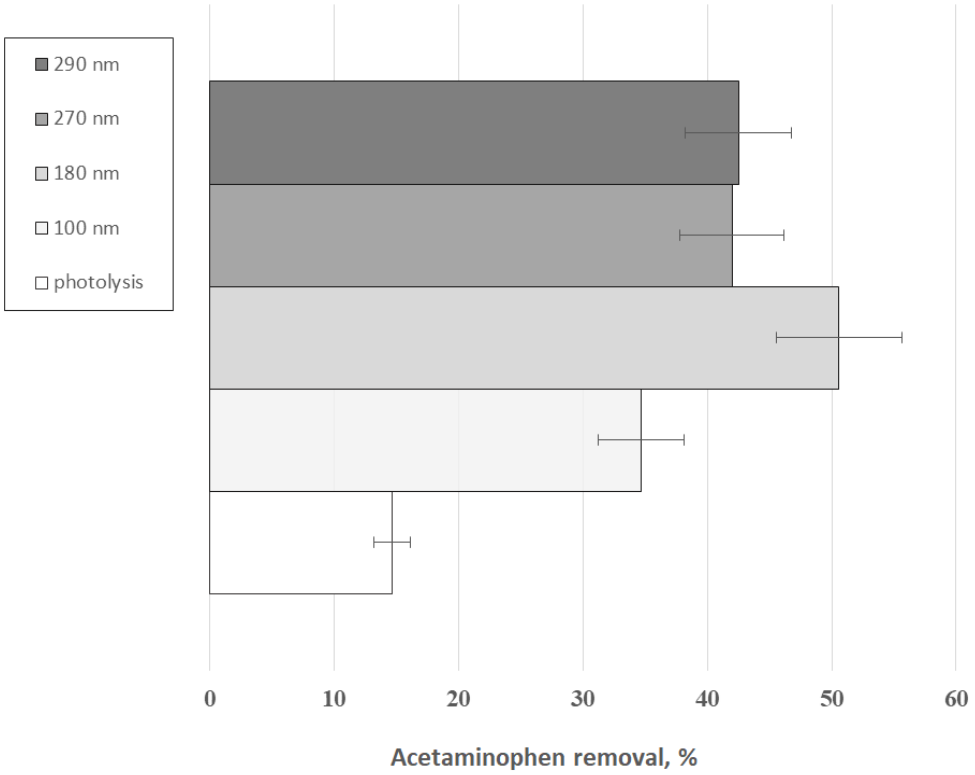


**Figure 9.** Effect of thickness of $TiO_2$ thin films deposited on smooth glass on removal of acetaminophen from model solution (UV dose 55 $Wh/m^2$)

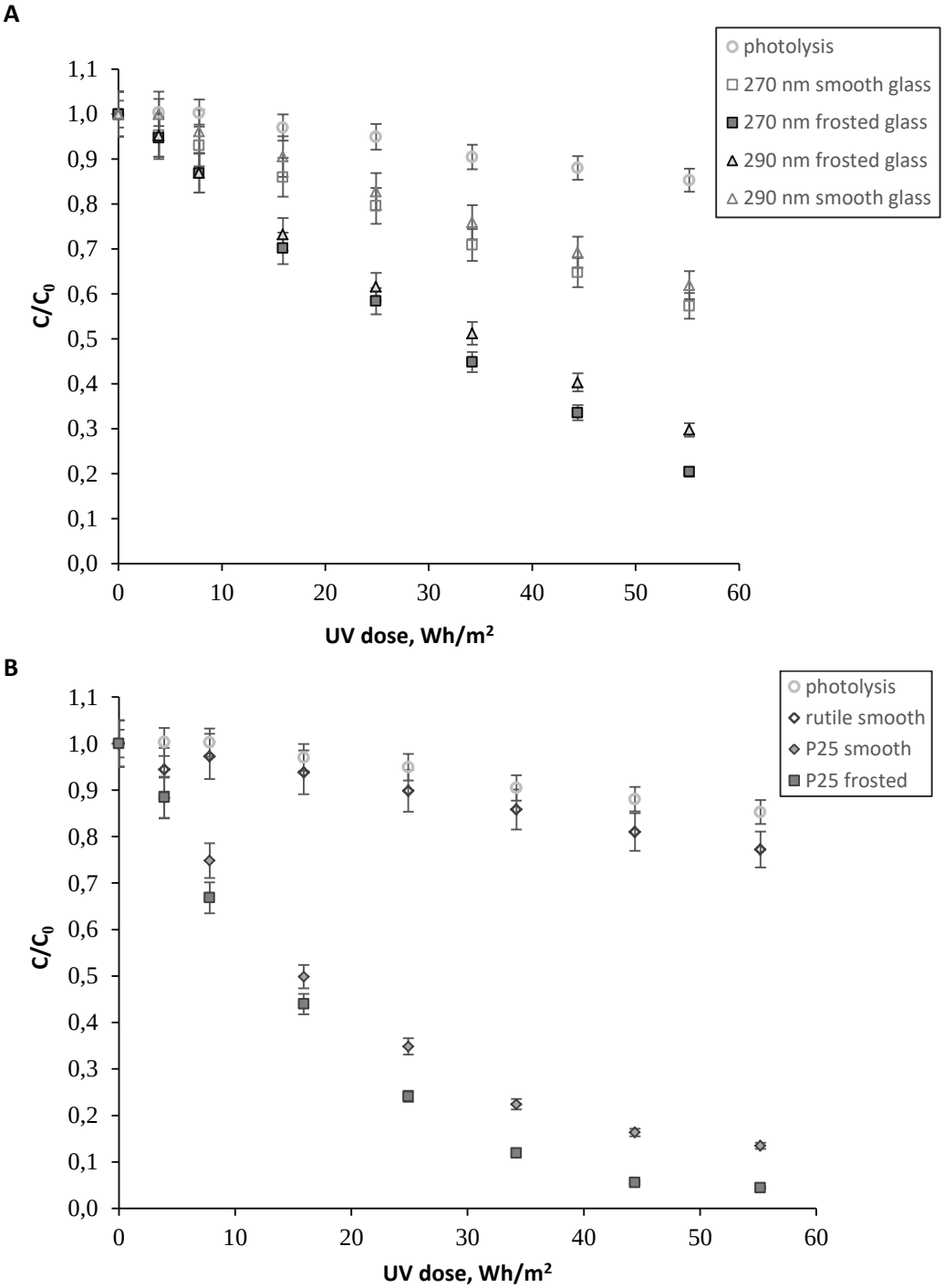


**Figure 10. A.** Degradation of acetaminophen using anatase thin films deposited on smooth and frosted glass tubes **B.** Degradation of acetaminophen using "sandwich" structure thin films deposited on smooth and frosted glass tubes

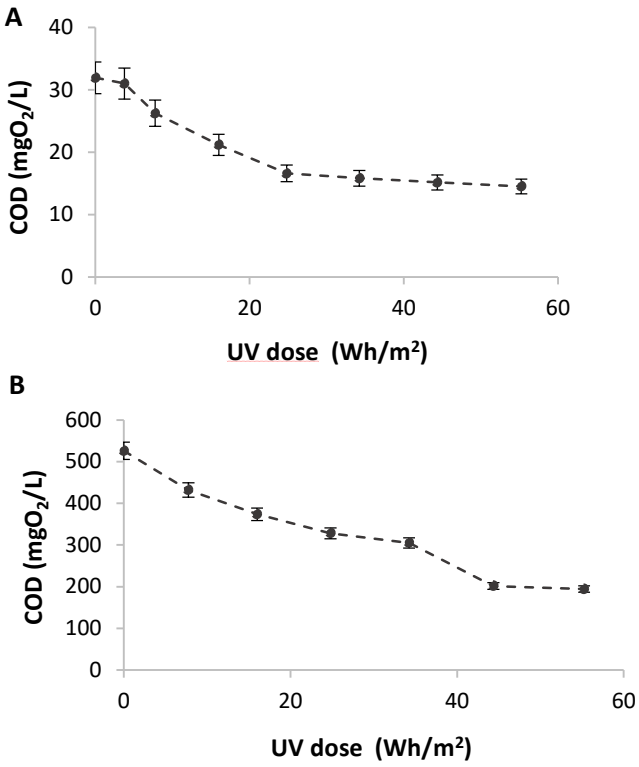


**Figure 11. A.** COD values during photocatalytic removal of acetaminophen from model solution under controlled irradiation conditions; **B.** COD values during photocatalytic removal of PhACs from urban wastewater effluent under controlled irradiation conditions

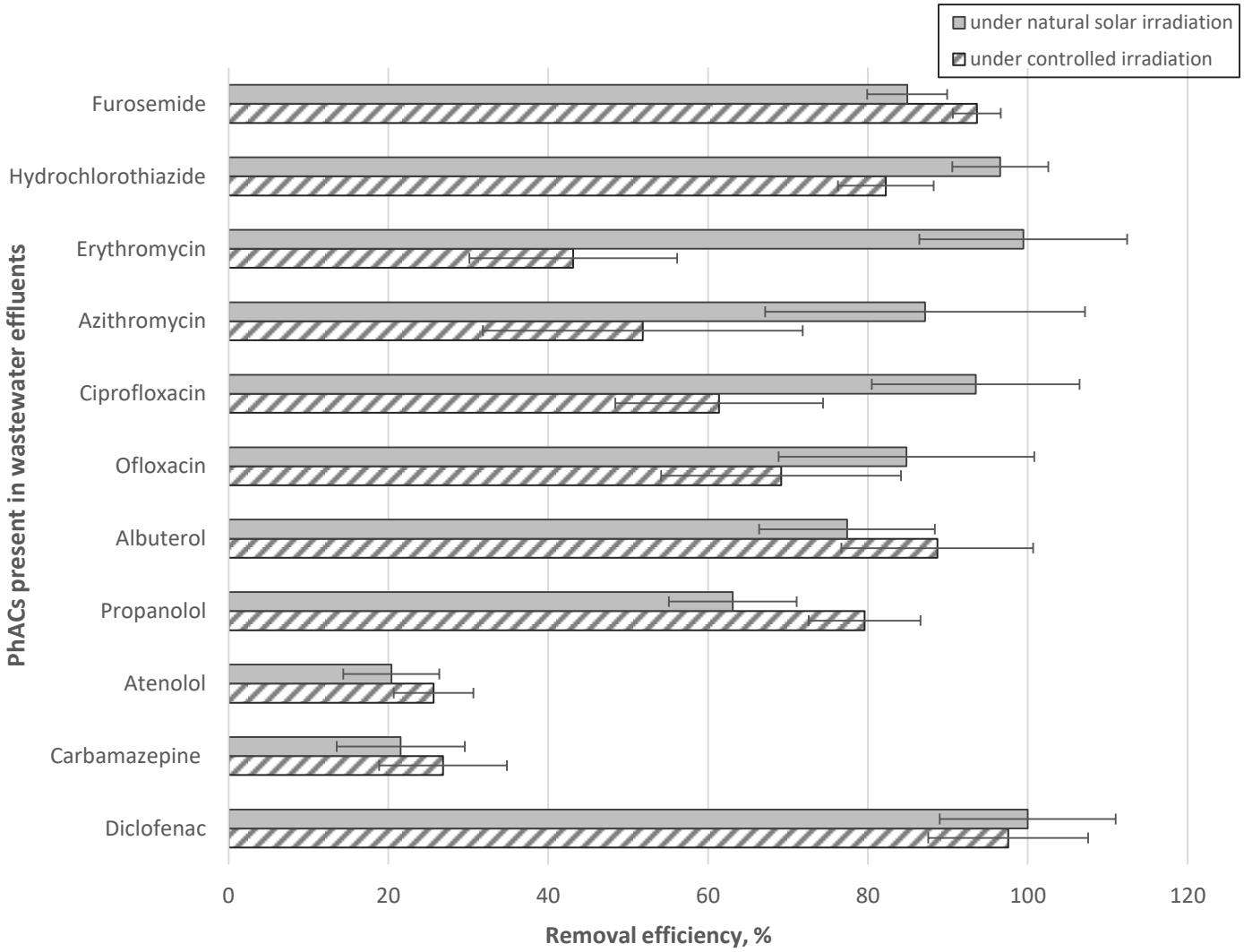


**Figure 12.** Efficiency of solar photocatalytic treatment for removal of PhACs from urban wastewater effluent under controlled irradiation (suntest, accumulated UV dose 55 Wh/m$^2$) and under natural solar irradiation (accumulated UV dose 33 Wh/m$^2$)

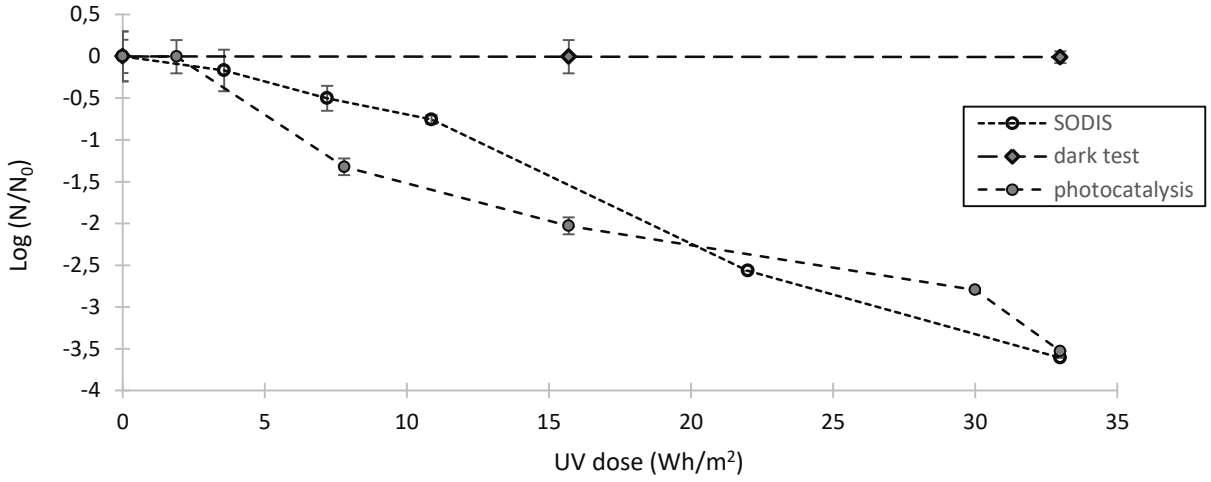


**Figure 13.** Inactivation of *E.coli* in wastewater effluents by solar disinfection (SODIS), solar photocatalysis and dark test (in absence of solar light and presence of photocatalyst)

**Table 1.** Characteristics of urban wastewater effluent (after filtration). Mean concentration of PhACs was measured in effluents used in experiments under controlled and natural solar irradiation

| **Parameter** | **Value** |
|---|---|
| pH | 7.46 |
| Conductivity, µS/cm | 1394 |
| COD, mg/L | 526.12 |
| **Pharmaceuticals** | **(suntest/solar)** |
| Diclofenac, ng/L | 792.4/ 611.3 |
| Carbamazepine, ng/L | 381.1/ 248.8 |
| Atenolol, ng/L | 1289.1/ 871.9 |
| Propanolol, ng/L | 14.7/ 10.3 |
| Albuterol, ng/L | 32.7/ 28.3 |
| Ofloxacin, ng/L | 316.3/ 155.5 |
| Ciprofloxacin, ng/L | 4862.6/ 3312.2 |
| Azithromycin, ng/L | 227.1/ 250 |
| Erythromycin, ng/L | 185.3/ 179.9 |
| Hydrochlorothiazide, ng/L | 5049.9/ 4005.4 |
| Furosemide, ng/L | 1369.7/ 870.6 |

**Table 2**. Initial disappearance rate of acetaminophen under controlled irradiation

| Type of photocatalyst | $k_{max}$ (mg $L^{-1}$ $m^2$ $Wh^{-1}$) | $R^2$ |
|---|---|---|
| photolysis | 0.036 | 0.98 |
| *anatase thin films deposited on smooth tubes* | | |
| 100 nm | 0.089 | 0.79 |
| 180 nm | 0.179 | 0.99 |
| 270 nm | 0.149 | 0.99 |
| 290 nm | 0.128 | 0.99 |
| *anatase thin films deposited on frosted tubes* | | |
| 270 nm | 0.264 | 0.99 |
| 290 nm | 0.227 | 0.98 |
| *"sandwich" structure films* | | |
| rutile | 0.083 | 0.97 |
| P25 on smooth tube | 0.505 | 0.98 |
| P25 on frosted tube | 0.767 | 0.98 |